40.0 EVALUATION OF PROCESSING PATH EFFECTS ON MICROSTRUCTURE AND PROPERTIES OF A POWDER-BASED AL-TM ALLOY.

Stuart Shirley (Mines)
Faculty: Kester Clarke (Mines)
Industrial Mentor: Rob Mayer (Queen City Forge)

This project initiated in Fall 2019. The research performed during this project will serve as the basis for a Master's thesis program for Stuart Shirley.

40.1 Project Overview and Industrial Relevance

As the aerospace and automotive industries continue to push the boundaries of fuel efficiency, the demand for lightweight, high-performance materials increases. Titanium and aluminum alloys are the primary metals used to meet the requirements of critical lightweight applications. In the commercial sector, the Boeing 747 is 68% aluminum and 4% titanium by weight; while fighter jets are 50% aluminum and 13% titanium by weight [40.1]. Clearly, titanium is utilized more broadly in critical applications where material cost can be justified. Over the operating lifetime of a fighter jet, material cost is approximately 2%, whereas 50% of the total lifetime jet cost is from operational costs, which are primarily from fuel usage [40.1]. To reduce operational cost, switching titanium parts to less dense aluminum will reduce the mass of the plane and increase fuel efficiency. Savings in fuel due to lightweight materials has become a critical factor in the automotive market as well in order to reduce CO_2 emissions [40.2].

Although titanium meets structural requirements at high temperatures, it is more costly and dense than aluminum [40.1]. Many current aluminum alloys begin to lose mechanical properties above 100 °C [40.1], and thus development of high temperature aluminum alloys is necessary when considering replacement of titanium with aluminum components. To this end, aluminum alloys with transition metal alloying elements (Al-TM) have been developed to retain high temperature mechanical properties [40.3]. Previous literature focused on the retention of ultimate tensile strength (UTS) in Al-TM alloys at elevated temperatures, up to ~350°C [40.4], is due to precipitate strengthening effects of the icosahedral phase found in this alloy.

Powder aluminum alloys are produced through gas atomization and subsequent consolidation. Gas atomization is a rapid solidification (RS) process that allows for great flexibility in composition and range of powder size of approximately 10-1000 μm [40.5,40.6]. Al-TM alloys produced through RS achieve a fine grain size of 4-5 μm [40.7] with further refinement achieved in consolidation [40.7,40.8] and extended solid solubility beyond the equilibrium value [40.9]. The decomposition of these supersaturated solid solutions increases the fraction of second phase particles formed during heat treatment [40.9], increasing the Orowan strengthening contribution. These fine second phase particles formed during RS are typically metastable [40.9] and transform to more stable equilibrium phases in the 400-500°C temperature range [40.9–40.11]. Additionally, the limited solubility of these phases at elevated temperature prevents coarsening. Thus, consolidation of these powders to a bulk form must be conducted via a solid-state process at relatively low temperatures or short times to retain second phase particles. Previous research on aluminum alloys with transition metals has been conducted primarily on melt-spun ribbons [40.11,40.12] and RS powders consolidated through extrusion [40.13]. This work seeks to further investigate Al-TM alloy microstructures produced by RS powder consolidated through extrusion and a solid-state friction-based processes.

Solid state processing paths for powder consolidation of interest include canned extrusion and friction stir extrusion. Canned extrusion requires multiple steps to achieve a consolidated bar from powder. Powder is first compacted into a can to increase density prior to extrusion and then sealed under vacuum to isolate the powder from the atmosphere [40.14]. Next, the canned powder is extruded through the die, with the can "jacketing" the extruded shape, from which the can is then removed [40.14]. The second process, friction stir extrusion, is related to shear assisted processing and extrusion (ShAPE): a solid-state method of powder consolidation. In this process, a rotating die is forced into a container of powder and the material back-extrudes through the center of the rotating die face [40.15]. Friction extrusion offers several advantages, including reduced processing time from powder to rod and improved

mechanical processing relative to traditional extrusion routes [40.7]. Additional thermomechanical processing via Gleeble® compression testing will be conducted as part of this project to develop understanding of forging effects on material produced by each of these processing pathways.

40.2 Previous Work

In the previous reporting period, DSC tests were conducted to determine the onset temperature of the exothermic peak associated with the transformation of the icosahedral phase [40.16]. An onset temperature of 520°C was observed, see **Figure 40.1**, in agreement with multiple sources citing a ~500°C exothermic peak as the transformation of the icosahedral phase [40.17]. To further corroborate these results, powder samples were quartz encapsulated under vacuum and heat treated at 460°C and 550°C for 30 minutes prior to X-ray diffraction (XRD). XRD has confirmed the transformation of the icosahedral phase to stable intermetallic phases following exposure to 550°C **Figure 40.2**.

An additional lower temperature exothermic peak at ~415°C, correlated to the formation of intermetallic precipitates, is reported for similar alloys [40.17]. In this study, DSC tests were unable to definitively detect the lower transformation around 415°C. However, XRD of powders following heating to 460°C begin transformation of the icosahedral phase to stable intermetallic phases, as observed in **Figure 40.2**. 460°C was used as an intermediate test temperature as the DSC peak reported by previous authors was a shallow and broad peak occurring over a wide temperature range and completed reaction around 460°C.

Previous work investigated thermal stability of an industrial 25:1 extrusion of Al-TM alloy via hardness testing following 100 hr holds at elevated temperatures. The study found an average room temperature hardness of 119 ± 1.7 μHV_{200}, and hardness decreased by 7 μHV_{200} when comparing as-produced material to samples held at 500°C [40.16] with further details in the previous report. After conducting thermal stability tests on similar alloy produced as melt spun ribbon, L. Sahoo and F. Audebert report a higher initial hardness and a drop in hardness of 150-200 µHV [40.11,40.18] when comparing as produced material to samples held at 500°C as shown in **Figure 40.3** with a decrease in hardness closely associated with the transformation of the icosahedral phase. XRD of the 25:1 extrusion revealed that the icosahedral phase had transformed to stable intermetallic phases during extrusion. The transformation of the icosahedral phase is likely responsible for the lower room temperature hardness, however the alloy maintained very consistent hardness up to 550°C after 100 hr.

40.3 Recent Progress

40.3.1 Powder Size Dependence of Icosahedral Phase

Previous work on alloys containing the icosahedral phase has shown a correlation between a reduction in powder size and an increase in the quantity of icosahedral phase [40.17]. The majority of literature has focused on powder sizes below 100 µm with higher concentration of the icosahedral phase [40.17- 40.20].

Utilizing DSC and XRD techniques outlined in the previous report [40.16], two distributions of powder size were investigated for the presence of the icosahedral phase. The fine powder size sample 136 has a D90 = 91µm and sample F01, containing larger powder particles, ranges from D10 = 112 µm to D90 = 215 µm.

A two-stage DSC test heating above the transformation temperature of the icosahedral phase is depicted in **Figure 40.4**. The transformation of the icosahedral phase is an irreversible exothermic reaction, in the first heating cycle of sample 136, plotted as a solid red line, an observable exothermic reaction occurs with an onset of ~520°C which is in good agreement with literature [40.17,40.21]. The second heating cycle of the same powder sample, plotted as the red dashed line, serves as a baseline to show that the reaction has completed and is irreversible. In complete contrast, the larger powder sample F01 displays little deviation between the two tests and no sign of an exothermic reaction. As expected these larger powder sizes do not contain a significant quantity of the icosahedral phase, with further confirmation via XRD.

Following the procedure outlined in **Section 40.2,** sample 136 and F01were heat treated at 460°C and 550°C. Resulting XRD scans in **Figure 40.2** depict the transformation of the icosahedral phase in sample 136 as outlined in previous reporting. Meanwhile the larger powder size sample F01 does not index icosahedral phase in the as atomized powder, see **Figure 40.5**, with no phase transformations occurring on heating of the powder corroborating the results from DSC. While it is difficult to prove the complete absence of the icosahedral phase within the tested powder of sample F01, if there is a quantity present it is of insufficient amount to be detected.

40.3.2 Production of Al-TM Extrusions

550-ton direct extrusions press at Michigan Technological University (MTU) consolidated Al-TM alloy over a range of extrusion temperatures and die ratios given in **Table 40.1**. In each extrusion condition, powder was loaded into an aluminum can to the packing density of the powder. The can was then attached to a vacuum pump and preheated in a fluidized bed to drive off moisture and achieve the target extrusion temperature. During the extrusion, the exit temperature was measured with a contact thermocouple and an IR pyrometer as shown in **Table 40.1**. Each extrusion condition resulted in consolidated and sound extrusions. Light optical and SEM investigation of representative samples from the center of each extrusion did not find porosity exceeding 100 µm, significantly smaller than the ASTM B211-20 class B indication. Samples for all further testing were sectioned away from the start and end of the extrusion to avoid unconsolidated material or intrusion of the 6061 can as shown in **Figure 40.6**.

40.3.3 Thermal Stability Testing

In continuation of the thermal stability testing from the previous reporting period, samples from the extrusions produced at MTU underwent 100 hr holds at temperatures of interest prior to hardness testing at room temperature **Figure 40.7**. The results are similar to previous work with an average room temperature hardness of 115 μHV_{200} and an average hardness decrease of 10 μHV_{200} when comparing as-produced material to samples held at 500°C. These results follow the expected trend, as the initial powder did not contain the icosahedral phase. Minor changes are evident in the microstructure of the extrusion following 100 hr at 550°C. In **Figure 40.8a**, oriented along the extrusion direction are regions of large intermetallic phases alternating with colonies of smaller phases in the as extruded condition. The disparity in intermetallic size is likely due to initial powder size with finer powder particles containing smaller intermetallic particles. **Figure 40.8b** shows a similar distribution of intermetallic particles following 100 hr hold at 500°C with minor coarsening.

8009 is another aluminum powder alloy designed for high temperature application and consolidated via extrusion. Sections of 8009 extrusion were subjected to the same testing discussed above, with hardness results also shown in **Figure 40.7**. The as extruded hardness test has not been completed due to equipment outages. The primary alloying additions to 8009 are iron, silicon, and vanadium, which form precipitates in the aluminum matrix upon the rapid solidification of the powder [40.22]. In **Figure 40.9a**, the as extruded condition shows a fine secondary phase dispersed in an aluminum matrix. Following the 550°C hold, these secondary phases coarsen significantly with large (20-30 µm) iron silicon leaf shaped intermetallic precipitates forming throughout the matrix, see **Figure 40.9b**, with this coarsening primarily responsible for the decrease in hardness.

40.4 Plans for Next Reporting Period

Plans for the next reporting period are outlined below.

- Thermomechanical testing: Gleeble® compression strain rate testing of extrusions
- EBSD grain size evaluation of extrusion microstructure from thermal stability tests

40.5 Acknowledgements

Kymera International provided Al-TM extrusions and powder for this research project. Special thanks to Tom Pelletiers and Wayne Daye for technical information and project support. AFSD billets are to be produced by research groups at Virginia Tech under Dr. Hang Yu and University of Alabama under Dr. Paul Allison. Friction extrusion (ShAPE) material was provided for this project by Scott Whalen, Pacific Northwest National Laboratories. Forgings and project support provided by Rob Mayer, Queen City Forge. Deform™ simulations provided by Suzanne Tkach, Tkach Metal Forming Consultants.

40.6 References

[40.1] A.P. Mouritz, Introduction to aerospace materials , Woodhead Publishing, Cambridge, England ;, 2012.

[40.2] J. Rowe, Introduction: advanced materials and vehicle lightweighting, in: Adv. Mater. Automot. Eng., Elsevier, 2012: pp. 1–4. https://doi.org/10.1533/9780857095466.1.

[40.3] S. Huo, W. Daye, F. Wolf, D.- Fürth, E. Wolfsgruber, New Generation PM Al-Materials for Automotive Applications, in: Eur. PM Conf. Proc., Shrewsbury: The European Powder Metallurgy Association, 2014.

[40.4] M. Galano, F. Audebert, A.G. Escorial, I.C. Stone, B. Cantor, Nanoquasicrystalline Al-Fe-Cr-based alloys. Part II. Mechanical properties, Acta Mater. 57 (2009) 5120–5130. https://doi.org/10.1016/j.actamat.2009.07.009.

[40.5] C. Schade, Introduction to Metal Powder Production and Characterization[1], Powder Metall. 7 (2015) 0. https://doi.org/10.31399/asm.hb.v07.a0006086.

[40.6] C. Schade, J.J. Dunkley, Atomization[1], Powder Metall. 7 (2015) 0. https://doi.org/10.31399/asm.hb.v07.a0006084.

[40.7] S.A. Whalen, M. Olszta, C. Roach, J. Darsell, D. Graff, T. Roosendaal, W. Daye, T. Pelletiers, S. Mathaudhu, N. Overman, High ductility aluminum alloy made from powder by friction extrusion, Materialia. 6 (2019). https://doi.org/10.1016/j.mtla.2019.100260.

[40.8] D. Vojtěch, J. Verner, J. Šerák, F. Šimančík, M. Balog, J. Nagy, Properties of thermally stable PM Al-Cr based alloy, Mater. Sci. Eng. A. 458 (2007) 371–380. https://doi.org/10.1016/j.msea.2006.12.136.

[40.9] A.V. Krainikov, O.D. Neikov, RAPIDLY SOLIDIFIED HIGH-TEMPERATURE Aluminum Alloys. I. Structure, Powder Metall. Met. Ceram. 51 (2012) 399–411.

[40.10] S. Pedrazzini, M. Galano, F. Audebert, G. Smith, Elevated temperature mechanical behaviour of nanoquasicrystalline Al93Fe3Cr2Ti2 alloy and composites, Mater. Sci. Eng. A. Struct. Mater. 705 (2017) 352.

[40.11] F. Audebert, F. Prima, M. Galano, M. Tomut, P. Warren, I. Stone, B. Cantor, Structural Characterisation and Mechanical Properties of Nanocomposite Al-based Alloys, Mater. Trans. 43 (2002) 2017–2025. https://doi.org/10.2320/matertrans.43.2017.

[40.12] M. Galano, F. Audebert, A.G. Escorial, I.C. Stone, B. Cantor, Nanoquasicrystalline Al-Fe-Cr-based alloys with high strength at elevated temperature, J. Alloys Compd. 495 (2010) 372–376. https://doi.org/10.1016/j.jallcom.2009.10.208.

[40.13] S. Pedrazzini, M. Galano, F. Audebert, P. Siegkas, R. Gerlach, V.L. Tagarielli, G.D.W. Smith, High strain rate behaviour of nano-quasicrystalline Al93Fe3Cr2Ti2 alloy and composites, Mater. Sci. Eng. A. 764 (2019) 138201. https://doi.org/https://doi.org/10.1016/j.msea.2019.138201.

[40.14] P. Samal, J. Newkirk, eds., Extrusion of Metal Powders, Powder Metall. 7 (2015) 0. https://doi.org/10.31399/asm.hb.v07.a0006085.

[40.15] N.R. Overman, S.A. Whalen, M.E. Bowden, M.J. Olszta, K. Kruska, T. Clark, E.L. Stevens, J.T. Darsell, V. V Joshi, X. Jiang, K.F. Mattlin, S.N. Mathaudhu, Homogenization and texture development in rapidly solidi fi ed AZ91E consolidated by Shear Assisted Processing and Extrusion (ShAPE), Mater. Sci. Eng. A. 701 (2017) 56–68. https://doi.org/10.1016/j.msea.2017.06.062.

[40.16] S. Shirley, K. Clarke, EVALUATION OF PROCESSING PATH EFFECTS ON MICROSTRUCTURE AND PROPERTIES OF A POWDER-BASED AL-TM ALLOY. CANFSA Report, Project 40, 2021.

[40.17] I. Todd, Z. Chlup, J.G. O'Dwyer, M. Lieblich, A. García-Escorial, The influence of processing variables on the structure and mechanical properties of nano-quasicrystalline reinforced aluminium alloys, Mater. Sci. Eng. A. 375–377 (2004) 1235–1238. https://doi.org/10.1016/j.msea.2003.10.209.

[40.18] K.L. Sahoo, I.C. Stone, Effect of Si on the formation and stability of the icosahedral quasicrystalline phase in Al-Fe-Cr-Ti alloys, Philos. Mag. Lett. 85 (2005) 231–245. https://doi.org/10.1080/09500830500218470.

[40.19] S. Pedrazzini, M. Galano, F. Audebert, D.M. Collins, F. Hofmann, B. Abbey, A.M. Korsunsky, M. Lieblich, A. Garcia Escorial, G.D.W. Smith, Strengthening mechanisms in an Al-Fe-Cr-Ti nano-quasicrystalline alloy and composites, Mater. Sci. Eng. A. 672 (2016) 175–183. https://doi.org/10.1016/j.msea.2016.07.007.

[40.20] A. Inoue, H. Kimura, High elevated-temperature strength of Al-based nanoquasicrystalline alloys, Nanostructured Mater. 11 (1999) 221–231. https://doi.org/https://doi.org/10.1016/S0965-9773(99)00035-5.

[40.21] M. Galano, F. Audebert, I.C. Stone, B. Cantor, Nanoquasicrystalline Al–Fe–Cr-based alloys. Part I: Phase transformations, Acta Mater. 57 (2009) 5107–5119. https://doi.org/10.1016/j.actamat.2009.07.011.

[40.22] D.J. Skinner, R.L. Bye, D. Raybould, A.M. Brown, Dispersion strengthened Al□Fe□V□Si alloys, Scr.

Metall. 20 (1986) 867–872. https://doi.org/https://doi.org/10.1016/0036-9748(86)90456-4.
[40.23] F. Audebert, R. Colaço, R. Vilar, H. Sirkin, Laser cladding of aluminium-base quasicrystalline alloys, Scr. Mater. 40 (1999) 551–557. https://doi.org/10.1016/S1359-6462(98)00459-X.

40.7 Figures and Tables

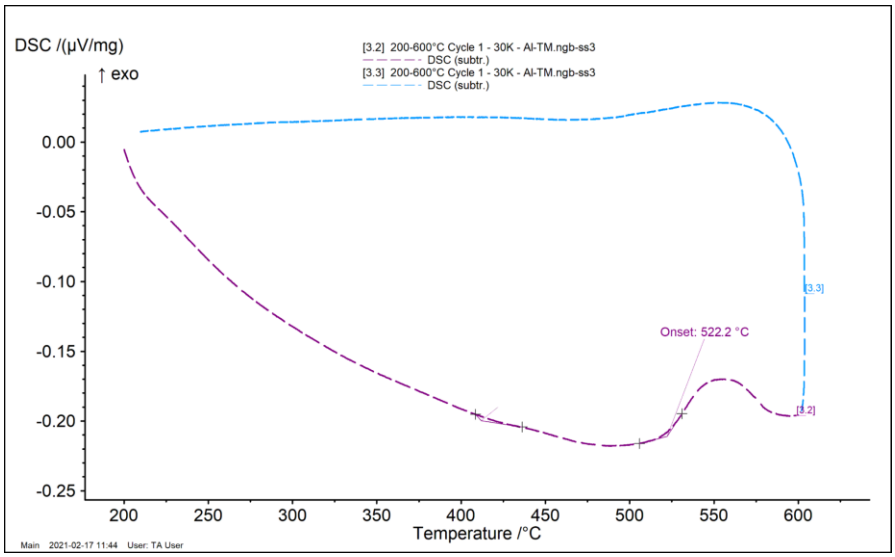

Figure 40.1: DSC of Al-TM powder test at a 30K/min heating rate from 200°C to 600°C, showing the onset of an exothermic peak at 520°C. The blue curve depicts cooling of the sample.

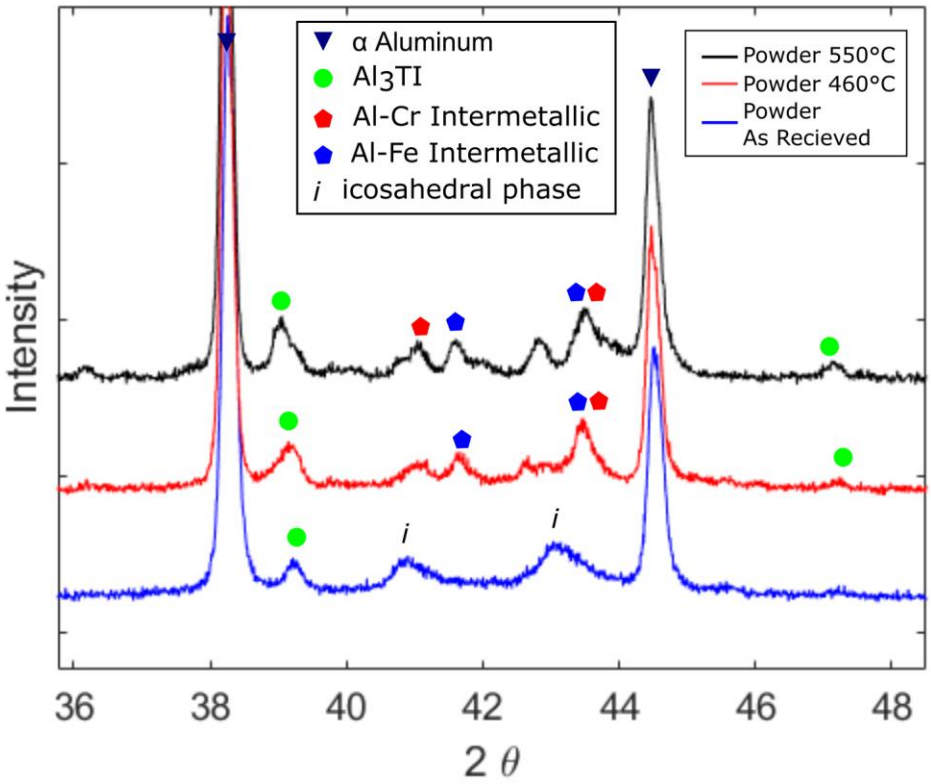

Figure 40.2: X-Ray diffraction 2θ range of 35 to 50° scans show in ascending order; Al-TM powder in the as-produced state (bottom, blue), Al-TM powder following 460°C hold with onset transformation to stable intermetallic phases (middle, red), and Al-TM powder following 550°C hold with complete transformation of the icosahedral phase to stable intermetallic phases (top, black).

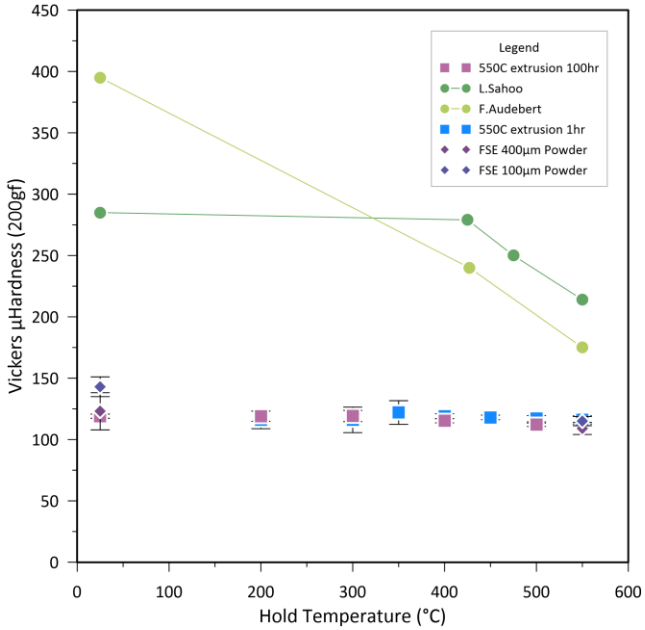

Figure 40.3: Al-TM Vickers hardness as a function of temperature. Average of 20 indents parallel to the extrusion direction after a 1 hr and 100 hr hold at temperature, all indents conducted at room temperature and denoted with square markers. Diamond markers are as-received hardness of Al-TM alloy consolidated through friction stir extrusion (FSE). Hardness of Al-TM alloy of interest denoted with round markers come from other studies on the alloy listed by first author [40.11,40.17–40.19,40.23].

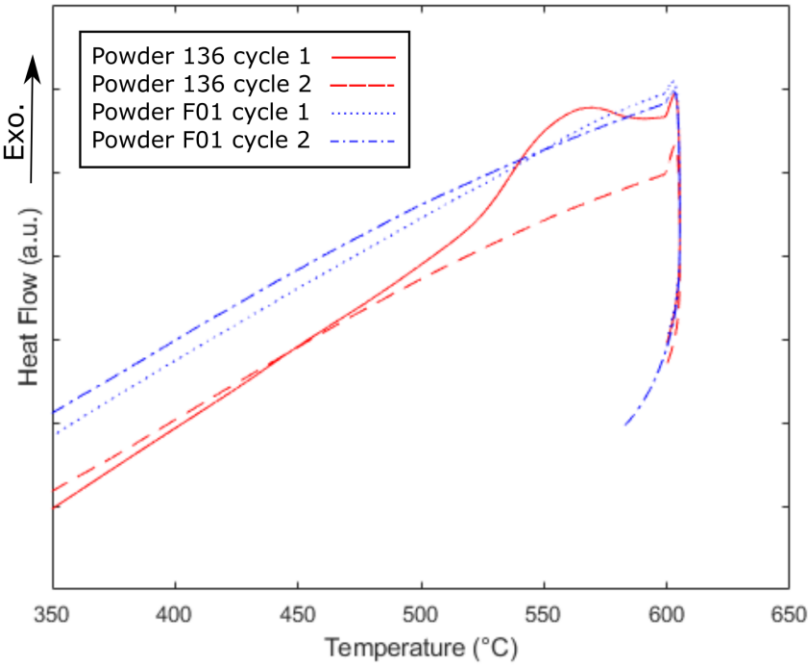

Figure 40.4: DSC of sample 136 (red) and F01 (blue), with a strong exothermic peak in the first run of sample 136 associated with the transformation of the icosahedral phase.

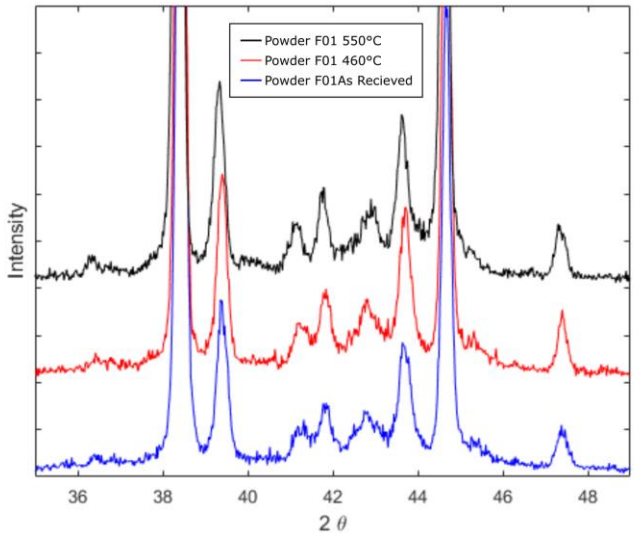

Figure 40.5: XRD 2θ range of 35 to 50°, XRD of the larger powder sample with no icosahedral phase present in the powder and maintaining secondary phases upon heating.

Figure 40.6: a) Representative extrusion, material between red lines used for testing. b) Cross section of extrusion near the end showing intrusion of 6061 can. c) Backscatter electron micrograph showing compositional contrast between 6061 (darker) and Al-TM (lighter) due to the higher content of Fe, Cr, and Ti in Al-TM leading to greater scatter of electrons back to the detector. Composition differences were confirmed with EDS line scans. d) Macro image of extrusion start where 6061 can failed at the start of extrusion, test specimens were extracted away from this region to avoid unconsolidated material.

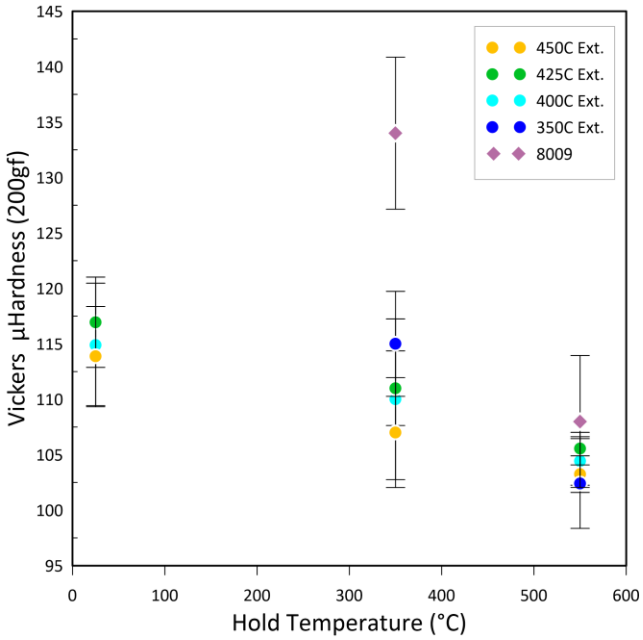

Figure 40.7: Al-TM extrusions listed by extrusion temperature and Vickers hardness as a function of hold temperature. Average of 20 indents parallel to the extrusion direction after 100 hr hold at temperature, all indents conducted at room temperature and denoted with round markers. 8009 shown in diamond, with higher hardness at 350°C, with hardness decreasing at 550°C due to coarsening of precipitates shown in **Figure 40.9**.

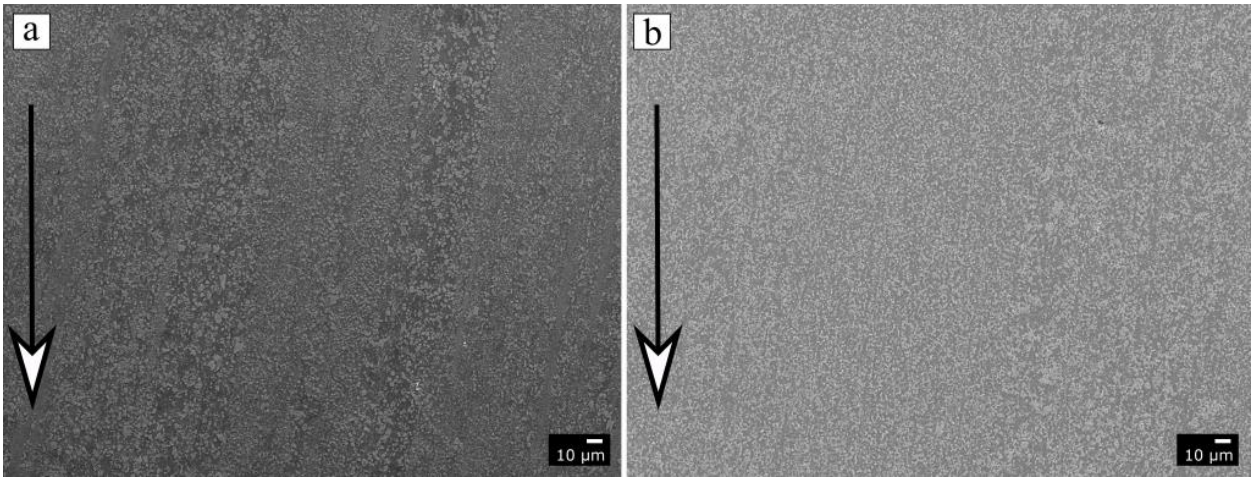

Figure 40.8: Al-TM 450°C extrusion condition with arrow indicating extrusion direction. a) SEM micrograph of as-extruded condition b) SEM micrograph of sample after 100 hours at 550°C hold showing minor coarsening of secondary phases.

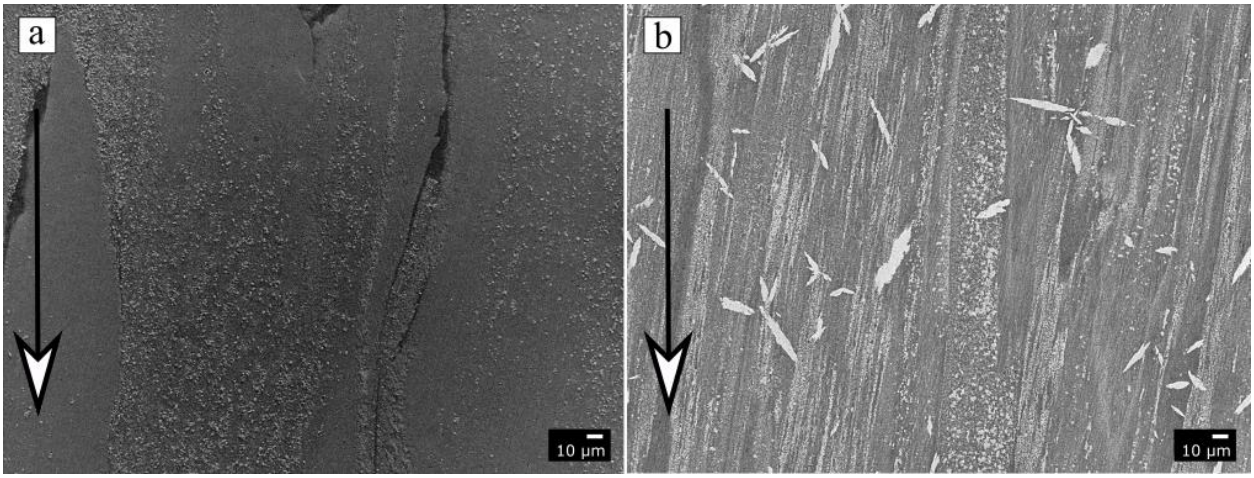

Figure 40.9: 8009 extrusion with arrow indicating extrusion direction. a) SEM micrograph of as extruded condition, the dark region parallel to the extrusion direction are regions of aluminum as determined by EDS b) SEM microgrpaph of sample after 100 hours at 550°C hold showing coarsening of secondary phases and precipitation of large leaf shaped FeSi dispersoids.

Table 40.1: Extrusion temperature and corresponding extrusion ratio with resulting exit temperatures of the extrudate. *Difficulties loading can into extrusion chamber, external thermocouple dropped 50°C before loading.

Extrusion Temperature (°C)	**Extrusion Ratio**	**Temperature Contact Thermocouple (°C)**	**Exit Temperature IR(°C)**
350	10:1	360	118
400	16:1	390*	420*
425	16:1	410	440
450	16:1	410*	440*